# Monitoring the polarization for the $A_1^n$ and $g_2^n$ experiments with the Compton polarimeter of the Jefferson Laboratory

Sébastien Binet

April 5, 2002

# Contents

# Chapter 1

# Introduction

During my master internship, I worked at the Jefferson Laboratory Hall A. I was in charge of the monitoring of the beam polarization during the $A_1^n$ (E99-117)[1][2] and $g_2^n$ (E97-103)[3][4] experiments. I also translated all the automatic logbook of the Compton polarimeter in the ROOT/C++ framework.

Jefferson Laboratory's accelerator can deliver up to 6 $GeV$ highly polarized electrons in a continuous beam at high current. The first beam came in 1997 (for Hall A) and since has provided a unique probe to study hadrons.

In this report, we are going to describe the Jefferson Laboratory and the target the experiment were using. Then we will explain the theoretical framework of the Compton Polarimeter. Afterwards, we will discuss the measurement of the polarization asymmetry and eventually we will show the results we got during the two experiments E99-117 and E97-103.

## 1.1 What is Jefferson Laboratory ?

In this section we will deal with the elements composing the accelerator. We will also explain briefly how it delivers polarized electrons to the three end stations (Halls A, B and C).

### 1.1.1 Elements of the accelerator

JLab is basically made of three parts : the injector, the linear accelerators (linac) and the three end stations where we can simultaneously run three different experiments.

The electron beam begins its first orbit at the injector and proceeds through the two linear accelerators (linac) joined by recirculation arcs. The accelerator uses super-conducting cavities to accelerate electrons. A cooling plant, called the Central Helium Liquefier provides liquid helium for ultra-low-temperature (4 $K$) super-conducting operations.

The electron beam can be split to be used by the three end stations. They are circular domed chambers called Hall A, B and C. Special equipments in each hall record the interactions between incoming electrons and a target.

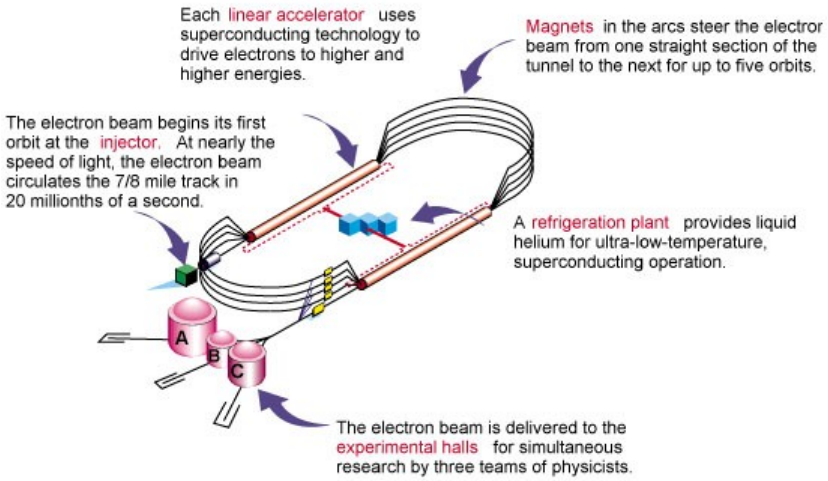


Figure 1.2: An overview of the JLab accelerator site.

### 1.1.2 The electron path

The electrons are extracted from a photo-cathode by illuminating it with a polarized laser light and are accelerated to about 45 *Mev* by an injector. They are then injected in the first linac, bent by $180^\circ$ in a recirculation arc, accelerated by the second linac and re-injected in the first linac by a second arc or sent to the halls. This cycle is called a pass and JLab can go up to 5 passes, each pass increasing the energy by the same amount. Each linac accelerates the beam by 400 to 500 $MeV$.

### 1.1.3 The electron source

The source of polarized electrons used is, in the current experiment, a strained GaAs crystal photo-cathode with theoretically 100% maximum polarization achievable. With this kind of source, the accelerator can deliver beam of around 80% polarization. We first took data with a 10 $\mu A$ current then at 12-15 $\mu A$ which is a good compromise between the target depolarization due to the beam, the radiation damage and the luminosity. Random 30 $Hz$ flips of the beam helicity cancel most of the systematics errors in asymmetry measurements that arise, for example, from beam current drifts, beam position drifts,...

A half-wave plate was periodically inserted at the source in the laser stream to reverse the helicity of the electron beam. This is used to check systematics

errors arising from helicity correlated electronic noise: the data taken with half-wave plate in and out must be consistent. In fact, when we insert or remove the beam half-wave plate, the polarization of the beam flips its sign but, in theory, not the systematic errors. Hence it is a way to check the systematic errors by subtracting the data with half-wave plate IN and OUT.

## 1.2 The Helium-3 polarized target

Both experiments of the summer 2001 were using polarized $^3He$ targets. We will explain such a choice and describe the geometry of those cells.

The main challenge when one wants to study neutrons is that free neutrons aren't stable (lifetime $\sim$ 15 $min$). On the top of that, we can't build a target of neutrons with a high luminosity. However we can use polarized $^3He$ as effective polarized free neutron target.

$^3He$ is made of a neutron and two protons. If the nucleus is in its ground state ($S$ state), the Pauli principle forces the protons to have spins of opposite signs and, as a matter of fact, the proton spin contribution to the $^3He$ one is cancelled. As a result, polarized $^3He$ targets can be seen as polarized neutron targets diluted in by two unpolarized protons. Protons will contribute to the nucleus' spin at second order due to the $D$-wave and $S'$-wave components of the ground state.

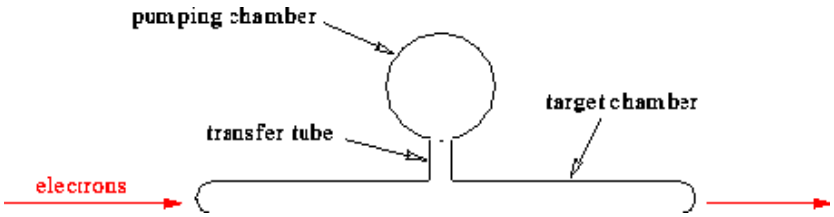


Figure 2: the Helium 3 polarized target.

Let us now discuss of the geometry of the cell.
A cell is made of two chambers (see Figure 2):

- The upper chamber, also called pumping chamber.
- The lower chamber (or target chamber), through which the beam will pass.

The cells we use at JLab are filled basically with $^3He$ and $Rb$. We use 25 $cm$ and 40 $cm$ target cells (resp for E99-117 and for E97-103) at approximately 10 $atm$ to achieve a high luminosity.

An important feature is the creation of a strong temperature gradient between the upper and the lower chamber. This gradient confines the $Rb$ in the upper chamber. Otherwise, the data we are interested in would be diluted by the Rubidium. To this end the upper chamber is placed in an oven heated to a temperature of $170 - 200^\circ$. We optically pump the $Rb$ gas thanks to 7 lasers of

30 $W$ (3 for longitudinal pumping and 4 for transverse pumping). The transfer of the polarization of the $Rb$ to the $^3He$ happens in the upper chamber, by spin exchange collision [5].

More than 40% target polarization was achieved with 10-15 $\mu A$ beam current. This polarization represents an equilibrium between the polarization efficiency (optical pumping) and depolarization processes (exposure to the beam, *He-He*, *He-Rb* and *He*-Cell interactions). The target can be polarized and kept polarized either into parallel or transverse mode thanks to the two sets of lasers and Helmholtz coils.

After this brief introduction of JLab, we will describe the Compton polarimeter apparatus in the next chapter.

# Chapter 2

# The Compton Polarimeter of JLab

## 2.1 Introduction

This chapter presents the Compton polarimeter of JLab and its components. We will see why it is useful to have an online measurement of the beam polarization. Furthermore, we will briefly explain the theory of the Compton scattering and how it can be used to yield to a polarization measurement. Afterwards we will explain the requirements to reach a good accuracy on the measurement.

The first polarimetry measurement of an electron beam have been performed in the early fifties after the first measurement of parity violation by C.S. Wu[6]. It is only in the 80's that some polarimeters based on Moeller or Compton scattering have been installed on linear accelerators.

The Compton polarimeter of JLab have been built by DAPNIA at Saclay, IN2P3/LPC of Clermont-Ferrand and Jefferson Laboratory. Its goal is to measure the longitudinal polarization of the electron beam delivered at JLab. It has been set up and installed in 1999 for the HAPPEX experiment.

## 2.2 The Compton polarimetry

In this section we will discuss the theory of Compton scattering. We will thus define all the useful parameters which are involved in the polarization measurement and how to extract polarization from the raw events.

The longitudinal polarization of an electron beam is defined as :

$$P = \frac{N^{\uparrow} - N^{\downarrow}}{N^{\uparrow} + N^{\downarrow}}$$

where $N^{\uparrow}$ (resp. $N^{\downarrow}$) is the number of electrons whose spin is aligned (resp. anti-aligned) with the beam direction.

At JLab, there are 5 polarimeters :

- 1 Mott polarimeter (located at the injector)
- 3 Moeller polarimeters (Hall A, B and C)
- 1 Compton polarimeter (Hall A)

### 2.2.1 Measurement principle

The Quantum Electrodynamic theory (QED) has been developed in 1950's. Klein and Nishina have been able to calculate the probability of the Compton scattering using QED. This process is now well known and may be used to measure other quantities such as the electron beam polarization.

For a Compton polarimetry measurement, we use the Compton scattering between a polarized electron beam and a circularly polarized photon beam in order to determine the polarization of the electron beam $P_e$ :

$$A_{exp} = \frac{N^+ - N^-}{N^+ + N^-} = A_{th} P_e P_\gamma \qquad \text{where} \quad A_{th} = \frac{\sigma^{\uparrow\Uparrow} - \sigma^{\downarrow\Uparrow}}{\sigma^{\uparrow\Uparrow} + \sigma^{\downarrow\Uparrow}}$$

$A_{th}$ is the Compton cross section asymmetry of the calculated polarized processes.

$P_\gamma$ is the photon beam polarization.

$\sigma^{\downarrow\Uparrow}$ and $\sigma^{\uparrow\Uparrow}$ are the cross sections for an anti-aligned (resp. aligned) electron scattering off an aligned (resp anti-aligned) target. Spins are projected on the the beam direction.

$N^+$ is the number of detected electrons with a spin aligned with the beam direction.

Let us notice that we have to use a polarized target because there is no asymmetry in QED for a polarized electron scattering off a non polarized target.

### 2.2.2 Compton scattering kinematic

In this two-body kinematic where the initial state is known, only one parameter is necessary to determine the whole kinematic (the angle $\Phi$ between the incident and scattered planes is not relevant at first order).

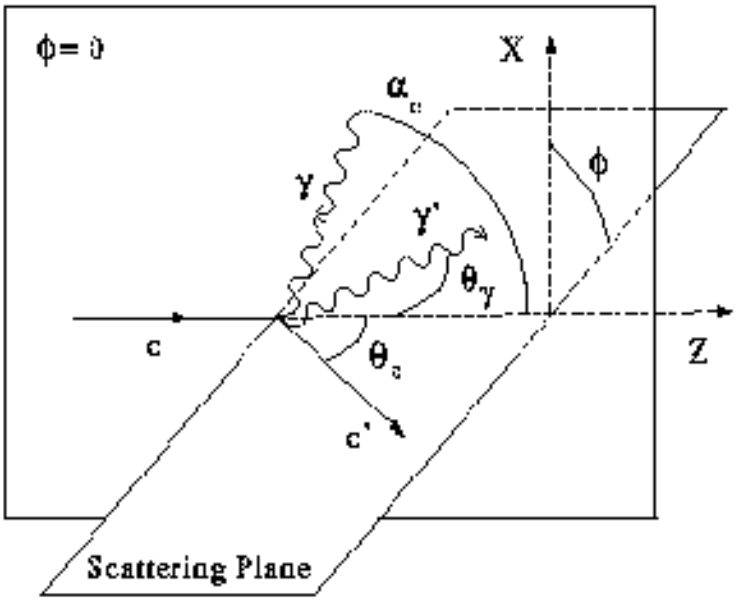


Figure 2.1: Compton scattering.

Applying the 4-momentum conservation in the lab frame $\left(\overline{p}+\overline{k}\right)^2 = \left(\overline{p}'+\overline{k}'\right)^2$, we can deduce the scattered photon energy which is linked to its scattering angle $\theta_\gamma$ by [8]:

$$\frac{k'}{k} = \frac{E + p\cos\alpha_c}{E + k - p\cos\theta_\gamma + k\cos(\alpha_c - \theta_\gamma)}$$

The small crossing angle approximation ($\alpha_c = 0$) yields

$$\frac{k'}{k} \simeq \frac{4a\gamma^2}{1 + a\theta_\gamma^2\gamma^2}$$

where $a = \dfrac{1}{1+\frac{4kE}{m^2}}$ (2.2.2) and $\gamma = E/m$.

- The maximal energy of the scattered photons $k'_{max}$ (the "Compton edge") is reached when $\theta_\gamma = 0$ and corresponds to the minimum of energy of the electrons $E_{min}$:

$$k'_{max} = 4ak\frac{E^2}{m^2}$$

$$E'_{min} = E - k'_{max} + k \qquad \Rightarrow E'_{min} \simeq E - 4ak\tfrac{E^2}{m^2}$$

- The minimum of energy of the photons $k'_{min}$ (and the maximal energy of the electron) is reached when $\theta_\gamma = \pi$ : $k'_{min} = k$ and $E'_{max} = E$.

Due to the large Lorentz boost along the beam direction, the photons will be emitted in a very small angle (*eg:* 300 $\mu rad$ for $E_e = 3.355\, GeV$ ). Thus we need a magnetic device to sort the incident and scattered beams of electrons and photons. This will be discussed in section 2.3.1.

### 2.2.3 Luminosity

One of the main parameter we have to care about is the luminosity. Indeed it drives the counting rates we can expect from the Compton interaction. Thus we will see in section 3.1.1 that a variation of this parameter induce a false asymmetry.

The total luminosity for the interaction of the laser and electron beam is :

$$\mathcal{L} = \int\int\int v_{rel}\rho_e\rho_\gamma dzdxdy$$

where $v_{rel}$ is the relative velocity of the two beams, $v_{rel} = c(1+\cos\alpha_c)$ and $\rho_e$ and $\rho_\gamma$ are the electron and photon beams' densities.

When the angular divergences of the electron and photon beams are small with regard to the crossing angle $\alpha_c$, the total luminosity can be approximated by integrating the differential luminosity over $z$. We get [8]:

$$\begin{aligned}\mathcal{L} &\simeq c(1+\cos\alpha_c)\frac{N_e^0 N_\gamma^0}{\sqrt{2}}\frac{1}{\sqrt{\sigma_e^2+\sigma_\gamma^2}}\frac{1}{\sin\alpha_c}\\ \mathcal{L} &\simeq \frac{1+\cos\alpha_c}{\sqrt{2\pi}}\frac{I_e}{e}\frac{P_L\lambda}{hc^2}\frac{1}{\sqrt{\sigma_e^2+\sigma_\gamma^2}}\frac{1}{\sin\alpha_c}\end{aligned}$$

where $I_e$ is the electron beam current, $P_L$ the laser power and $\lambda$ the laser wavelength.
A high luminosity for non zero crossing angle depends on the ability to obtain small and comparable beam spot sizes and small crossing angle. At JLab, the electron beam spot size is usually around $100\,\mu m$ and we can see it with the so called "Bell curve" (see section 3.2).

### 2.2.4 Cross section

Let $\rho$ be the ratio of momentum carried by the photon over the maximal energy:

$$\rho = \frac{k'}{k'_{max}}$$

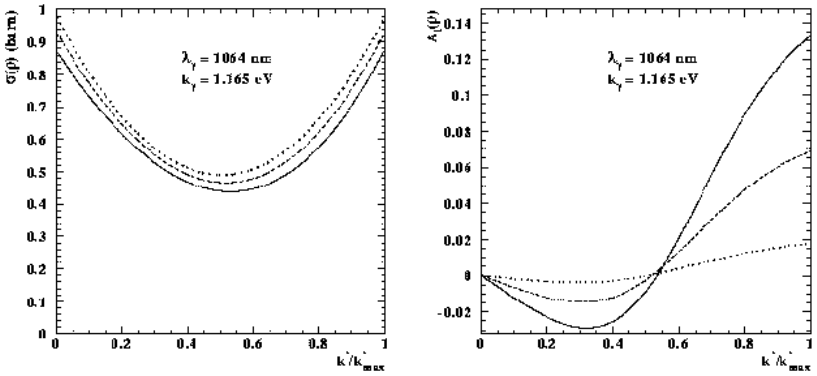


Figure 2.2: On the left is plotted the cross section of the Compton scattering for different electron energies. The right graph shows the theoretical asymmetry for different incident electron energies. (Solid line for E=8 $GeV$, dashed line for E=4 $GeV$ and dotted line for E=1 $GeV$)

The cross section for $\alpha_c = 0$ and each electron polarization state is [7]:

$$\frac{d^2\sigma_c^{\pm}}{d\rho d\Phi} = \underbrace{\frac{d^2\sigma_0}{d\rho d\Phi}}_{\substack{\text{non polarized} \\ \text{Compton cross section}}} \mp \left[ \underbrace{\cos\theta \frac{d^2\sigma_1}{d\rho d\Phi}}_{\substack{\text{longitudinal Compton} \\ \text{cross section}}} + \sin\theta\cos\Phi \frac{d^2\sigma_2}{d\rho d\Phi} \right]$$

$\theta$ = angle between the polarization vector and beam axis
$\Phi$ = azimuthal angle

$$\begin{aligned}
\frac{d^2\sigma_0}{d\rho d\Phi} &= ar_0 \left[ \frac{\rho^2(1-a)^2}{1-\rho(1-a)} + 1 + \left( \frac{1-\rho(1+a)}{1-\rho(1-a)} \right)^2 \right] \\
\frac{d^2\sigma_1}{d\rho d\Phi} &= ar_0 \left[ (1-\rho(1+a)) \left( 1 - \frac{1}{(1-\rho(1-a))^2} \right) \right] \\
\frac{d^2\sigma_2}{d\rho d\Phi} &= ar_0 \left[ \frac{\rho(1-a)\sqrt{4a\rho(1-\rho)}}{1-\rho(1-a)} \right]
\end{aligned}$$

where $r_0 = 2,82.10^{-13}\,cm$ is the classical radius of the electron and $a$ is defined page 11.

Due to the Lorentz boost, all the events are detected in the same element of detection. As a consequence, our detector setup covers the whole azimuthal angle:

$$\int \frac{d\sigma_c^{\pm}}{d\rho d\Phi} d\Phi = \frac{d\sigma_0}{d\rho} \mp \frac{d\sigma_1}{d\rho} \cos\theta$$

### 2.2.5 Relative cross section asymmetry

Cross section asymmetries are convenient to get a polarization measurement because they are easier to measure than absolute cross sections.

Let $A_{th}$ be the relative asymmetry of the longitudinal Compton cross section:

$$A_{th} = \frac{\frac{d\sigma_c^+}{d\rho} - \frac{d\sigma_c^-}{d\rho}}{\frac{d\sigma_c^+}{d\rho} + \frac{d\sigma_c^-}{d\rho}} = \frac{\frac{d\sigma_1}{d\rho}}{\frac{d\sigma_0}{d\rho}}$$

The Compton asymmetry flips its sign for:

$$\rho_0 = \frac{1}{1+a} = \frac{1}{2}\frac{1+\frac{4kE}{m^2}}{1+\frac{2kE}{m^2}}$$

and its maximal value goes from 1% to 10% at the JLab energies:

$$A_{th}^{max} = A_{th}(k'_{max}) = \frac{1-a^2}{1+a^2}$$

The Compton asymmetry is negative for low-energetic scattered photons and positive for energetic photons. This detail will be important for the minimization of the measurement time. Indeed if put a very low threshold it decreases the asymmetry because of the negative part of the asymmetry. Hence it decreases the statistical accuracy on the error.

### 2.2.6 Getting a polarization measurement

The asymmetry counting rate measured in our detector depends on the luminosity, the Compton cross section, the measurement duration and the efficiency of our detector at given energy, as follow :

$$N^{\pm}(E) = \mathcal{L}^{\pm}\sigma_c^{\pm}(E)T^{\pm}\epsilon^{\pm}$$

where $T$ is the time of measurement and $\epsilon$ is the detector efficiency.

If the parameters are independent of the beam polarization state, then the experimental asymmetry measurement of the counting rate $A_{exp}$ allows us to determine the electron longitudinal polarization :

$$A_{exp} = \frac{N^+ - N^-}{N^+ + N^-} = P_e^{||} P_\gamma \langle A_{th} \rangle$$

where $P_e^{||}$ is the longitudinal polarization of the electron, $P_\gamma$ is the photon polarization and $\langle A_{th} \rangle$ is the analyzing power of the longitudinal Compton cross section.

#### Analyzing power

The analyzing power is the convolution of the detector efficiency (the smeared function of our detector) and the physics of the process.

The average value of the experimental asymmetry weighted by the total non-polarized cross section is:

$$\langle A_{th} \rangle = \frac{\int_{\rho_{min}}^1 \epsilon(\rho)\frac{d\sigma_0}{d\rho}(\rho)A_{th}(\rho)d\rho}{\int_{\rho_{min}}^1 \epsilon(\rho)\frac{d\sigma_0}{d\rho}d\rho}$$

where $\rho_{min}$ is the detection threshold of the Compton photons and $\epsilon(\rho)$ is the detector efficiency. $A_{th}$ is perfectly determined from QED once the kinematics parameters of the process are known (*eg* energy of the electrons and the photons).

If $\rho_{min} = 0$, $< A_{th} >$ is the theoretical cross section asymmetry. We will now refer to this quantity by analyzing power of the polarimeter.

## 2.3 The experimental device

First of all, let us notice that the beam characteristics at JLab makes polarimetry measurement by Compton scattering challenging:

- the asymmetry is low compared to other accelerators : SLAC reach $\sim 75\%$ with regard to $\sim 1.5\%$ at JLab for a beam energy of 4 $GeV$ and a photon beam energy of 1.165 $eV$.
  As a consequence we need more time or higher photon flux to reach the same relative statistical accuracy as SLAC.

- the intensity delivered at JLab is "low" ($< 100\,\mu A$), compared to the available current in a storage ring ($\sim mA$).

Therefore we have to increase the luminosity by maximizing the power of the laser using an optical cavity and the laser polarization.

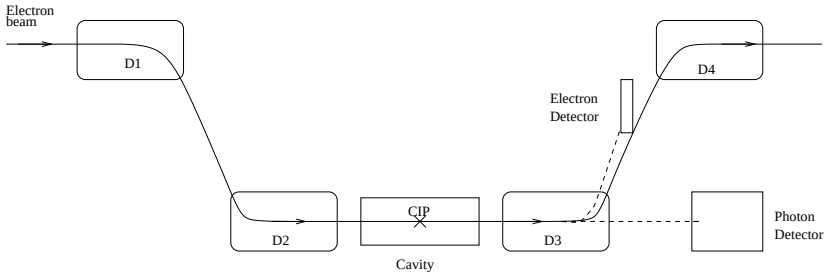


Figure 2.3: The complete device of the Compton polarimeter. We can notice the four coupled dipoles, the optical Fabry-Perot cavity and the electron and photon detectors. Let us notice that it was the first time a cavity was coupled with an accelerator.

### 2.3.1 Magnetic chicane

As noticed previously, the electrons and photons are emitted in a very small opening angle ($< 300\,\mu rad$).

Consequently we need to sort the incident and scattered beams. It is performed by a magnetic chicane composed of 4 identical dipoles: the dipoles have the same field integral ($\pm 10^{-5}\,T$). It allows us to perform non destructive

sorting because the total field integral equals zero. Hence it is a non invasive measurement.

Each magnet generates a magnetic field of amplitude up to 1.5 $T$. This allows to pass an electron beam of maximal energy of 8 $GeV$. The supply of each dipole is coupled in series. Therefore, changing the current in the current supply results in modifying the vertical position of the electron beam between the $D_2$ and $D_3$ dipoles. This allow us to perform a vertical sweep of the beam at the Compton interaction point (CIP) without modifying the position and the angles of the beam on the main experiment target. That way we can optimize the crossing between the electron and photon beams in order to maximize the luminosity at the CIP and also reduce our sensibility to false asymmetries which could arise (see section 3.1.1).

### 2.3.2 The vacuum

One of the main factor contributing to the background in the electron and photon detectors is due to the residual vacuum. The electron of the beam can do Bremsstrahlung on a molecule of the gas and hence simulate a photon and an electron coming from a Compton interaction. That is why a good vacuum is required.

The vacuum is established thanks to 5 pumps :

- a primary pump which decreases the pressure down to $10^{-4}\,Torr$
- 4 ionic pumps of $120\,l.s^{-1}$ which decrease the pressure down to $10^{-8}\,Torr$ in the central section, between the second and the third dipoles ($D_2$ and $D_3$)

The residual vacuum is mainly composed of molecules of hydrogen (74%), water (19%), nitrogen (5%) and helium (2%).

With such vacuum, we can limit the Bremsstrahlung background to lower than 1 $kHz$ for an electron beam intensity of 100 $\mu A$ and an energy of 4 $GeV$. This background corresponds to 1% of the counting rates (without the background due to the halo).

### 2.3.3 The beam diagnostic scintillators

During the first use of the Compton polarimeter, the background measured in the detectors was a thousand timer higher than expected ($\sim MHz$ instead of $\sim kHz$). It appeared that it was due to the electrons of the halo which were scrapping onto the mechanical supports of the cavity mirrors which have an apparture of $\sim 5\,mm$ along the x axis and around 5 $cm$ along the y axis. Hence the focusing and the position of the electron beam upstream the CIP is very important.

Four sets of scintillators have been installed to monitor the beam tuning:

- one upstream the chicane.

- one before $D_2$.
- on both sides of the optical table, between $D_2$ and $D_3$.

When the beam is mistuned, the counting rates in these scintillators increase. Therefore, the optimization of the beam tune is done by minimizing these signals. Moreover, we can also check this tune by monitoring the counting rates in the photon detector when the cavity is OFF.

### 2.3.4 The photon source

In order to minimize the time of measurement, we have to :

- maximize the laser power,
- maximize the photon polarization ($\pm 100\%$),
- maximize the overlap of the transverse sections laser beam - electron beam,
- minimize the crossing angle $\alpha_c$.

During a run, we have also to measure the polarization (*cf* page 14) of the laser inside the cavity as well as its power. Indeed, if we increase the power of the laser, we increase the counting rates too. So, this parameter comes into the calculation of the statistical error bar.

#### The principle of the Fabry-Perot cavity

Because of the lack of room near the chicane, it is not possible to use large power laser. As a consequence, a low power laser (200 $mW$) amplified by a resonant Fabry-Perot cavity have been installed.

We couple a photon source with a cavity composed of two ultra-reflecting mirrors. The distance between the two mirrors ($L$) defines the resonant frequency of the cavity:

$$\nu_{cav} = \frac{c}{2L}$$

If the incident wave has a wavelength equal to a multiple of $\nu_{cav}$ , constructive interferences between incident and resonant waves are built inside the cavity. As a result, the intra-cavity power is being increased.

The mirrors presently in use have been built by the "Service des Matériaux avancés" of the IPN Lyon. They are made of several layers of $SiO_2$, $Ta_2O_5$ and $Si$. They reach a reflectivity $R = 99,988\%$ and a transmitivity $T = 95\,ppm$.

Hence, the maximum gain $G_{max}$ defined as [7]:

$$G_{max} = \frac{T}{(1-R)^2}$$

can be as great as 7500. So, for a IR laser beam of 200 $mW$, we can reach a power of 1500 $W$ at the CIP with new mirrors. Indeed, because of radiation damage, mirrors are being altered (ionization of the different layers composing them resulting in a lifetime of a few years).

### 2.3.5 The photon detector

#### Constraints on the detector

With an electron beam of 4 $GeV$ and 100 $\mu A$ and a laser power of 1500 $W$, the photon detector runs at a counting rate[8] of 100 $kHz$.

The measurement of the energy $E_\gamma$ of the scattered photon must be done in less than 100 $ns$ to avoid the pile-up which could skew our measurement. Moreover, the detector is located downstream the third dipole $D_3$ where there is room constraint: the crystal must have the smaller Moliere radius in order to contain the whole shower and allow a measurement of the total energy $E_{tot}$ of the photons. These conditions are filled by the $PbWO_4$ crystal making the calorimeter[11]. The photon detector is composed of a $5 \times 5$ matrix of crystals of $2 \times 2 \times 23\, cm^3$. The generated light is read by small photo-multipliers Philipps XP1911.

Let us notice that the radiation length of the $PbWO_4$ is 0.92 $cm$[12]. Hence all the shower is detected in the longitudinal direction.

But, even if the $PbWO_4$ crystal has high detection performances, it can be blind by the synchrotron radiations induced by the chicane.

#### Background for the photon detector

The radiations to be considered here are the synchrotron photons emitted by the $D_2$ and $D_3$ dipoles.

A thick collimator is mounted on the calorimeter. It consists in a big plate of lead with a hole of radius $r_\gamma = r_c + 2\, mm$ where $r_c$ is the spot size of the scattered photons at the calorimeter position. This shields the detector from undirectional and low energy bremsstrahlung. A thin absorber made of inox is put in front of the hole. Therefore it decreases the synchrotron background because the cross section of the synchrotron radiation is high at low energy.

### 2.3.6 The electron detector

Since the Compton scattering is a two-body interaction, the knowledge of the parameters of only one scattered particle is enough to determine the whole kinematics. However, the electron detector allows us to calibrate the photon detector and also to perform an independent measurement.

The electron detector allows us to reduce the systematic error on the polarization measurement by determining the momentum of the scattered electron and hence the scattered photon: we measure its deviation through the third dipole magnet. Let us notice that the electron detector has a really good energy resolution because of its ability to reconstruct the path of the incoming electron.

Therefore, we will be able to take data with the electron detector only, with the photon detector only or with the two in coincidence (for intercalibration of the two detectors).

### Principle of the measurement

To reduce radiation damage due to synchrotron radiation, the detector is located between $D_3$ and $D_4$.

The final position ($41\,cm$ after $D_3$) is a compromise between the maximum dispersion and the space left for the vacuum pipe used when the magnetic chicane is not used. Let $L_3$ be the length of $D_3$ and $l_e$ the distance between the end of that dipole and the electron detector. For an electron of momentum $p'$, the transverse deviation $d'$ at the electron detector location is [8]:

$$d' = R(1 - \cos\theta) + l_e \tan\theta$$

with $\sin\theta = \frac{0.3\,B(T).L_3(m)}{p'(GeV)}$ and $R(m) = \frac{p'(GeV)}{0.3\,B(T)}$.

The electron detector must be kept out of the main beam with a minimum safety gap $Y_{det} \sim 5-6\,mm$. The corresponding energy $E_{gap}$ will be the maximal measured energy of the scattered electron and fix the energy threshold on the scattered Compton photon.

### Description of the detector

The electron detector consists of 4 planes of silicon strips in order to have a high efficiency with a good rejection of accidental coincidences and non-directional background. The main feature of coupling a microstrips based detector to a dipole is to measure the energy of the particle detected, knowing its path. The path of the scattered electron is known using a tracking algorithm.

Each plane is composed of 48 strips of $600\,\mu m$ width and $200\,\mu m$ thickness. The gap between 2 strips is $50\,\mu m$. The size of a plane in the dispersive direction is $3.2\,cm$.

The useful size of the detector is $d_{min} - Y_{det}$ and decreases with low energies. This size is thus maximal for $E = 8\,GeV$.

The effects of the smearing due to the finite resolution have to be corrected and the errors on the different parameters governing this resolution (beams interaction size and resolution on the magnetic dispersion) are propagated into systematic errors.

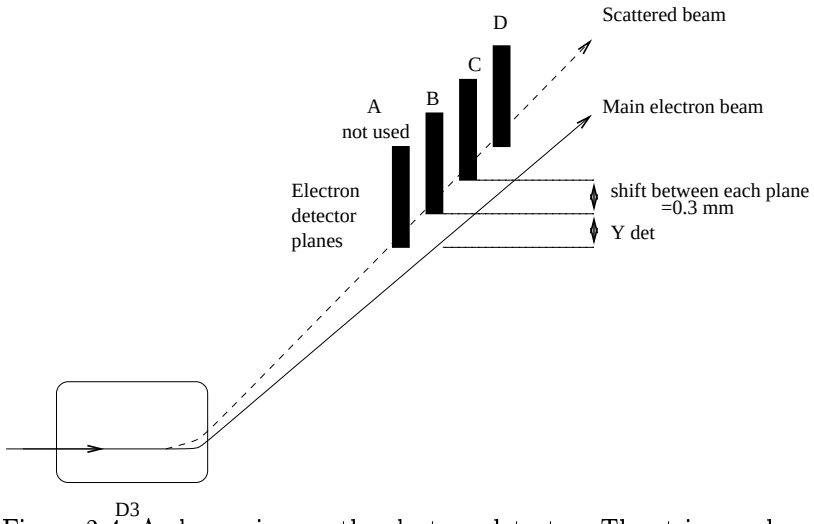


Figure 2.4: A closer view on the electron detector. The strip number is increasing with the dispersion direction.

The total transverse deviation $d'$ for an electron of momentum $p'$ after a dipole (length $L$, field $B$) and a drift (length $l$) is, for a perfect dipole and neglecting the incident electron angle [8]:

$$\begin{aligned} d' &= R(1-\cos\theta) + l.\tan\theta = R\sin\theta\tan\tfrac{\theta}{2} + l\tan\theta \\ &= \sin\theta\left(\tfrac{L}{1+\cos\theta} + \tfrac{l}{\cos\theta}\right) \end{aligned}$$

where $\theta$ is the deviation angle and $R$ the radius curvature of the scattered electron trajectory. For a small deviation angle $\theta$, the transverse deviation can be approximated by:

$$d' \simeq \sin\theta\left(\frac{L}{2}+l\right) \simeq \frac{0.3\,BL}{p'}\left(\frac{L}{2}+l\right) \simeq \frac{A}{p'}$$

The displacement $\Delta y$ for an electron of momentum $p'$ from one of the beam of momentum $p$ is given by:

$$\Delta y = d' - d = \frac{A}{p'} - \frac{A}{p} = -\frac{A}{p}\left(\frac{p'-p}{p'}\right) = \alpha\frac{\Delta p'}{p'}$$

and depends on the dispersion $\alpha$. Let us notice that the displacement depends on the energy of the scattered electron. The displacement $\Delta y$ can be known with a high accuracy because of the thin width of the strips and the little gap between each one.

The energy $k'$ of the scattered photon is then measured by the displacement $\Delta y$ of the scattered electron (momentum $p' = p - k'$, with the incident photon energy neglected) through $\Delta y = \alpha\frac{\Delta p'}{p'}$ with $\Delta p' = p' - p = -k'$ :

$$k' = p\frac{\Delta y}{\Delta y - \alpha}$$

Thus the resolution on the photon energy $k'$ is given by :

$$\frac{\sigma(k')}{k'} = \frac{\sigma(p)}{p} \oplus \sigma(\Delta y)\frac{(p-k')^2}{\alpha p k'} \oplus \sigma(\alpha)\frac{p-k'}{\alpha p}$$

It is due to :

- the energy resolution of the beam $\sigma(p)$ .
- the transverse size of the interaction between the laser beam and the electron beam $\sigma(\Delta y)$. This size is close to 100 $\mu m$ and has to be known with an accuracy of 50 $\mu m$ .
- the resolution on the dispersion $\sigma(\alpha)$ which includes higher order magnetic effects neglected in the parameterization of the dispersion and the angular divergence of the electron beam and scattering angle of the Compton electron.

**Note :** The energy resolution of the beam $\sigma(p)$ can be neglected here.

**Bremsstrahlung for the electron detector**

The bremsstrahlung seen by the electron detector is due to [8]:

- bremsstrahlung photons generated between the end of $D_3$ and the electron detector. The useful length is only $L \simeq 3.6\,m$ and the photons are seen under an angle $\theta > 1.4\,mrad$ larger than the characteristics bremsstrahlung angle $\theta_{brem} \simeq m/E < 0.25\,mrad$. So this background is very weak compared to the Compton rate.
- electrons having emitted a bremsstrahlung photon between the dipoles 2 and 3 and with an energy in the energy range $[\rho_{min}, \rho_{max}]$ covered by the electron detector. The useful length for bremsstrahlung is the same ($L \simeq 2.5\,m$) than for the photon detector.

Outgoing bremsstrahlung electrons are emitted with angles $\theta \simeq \frac{1}{\gamma} = m/E$. These angles are small ($\theta < 0.25\,mrad$) and can be neglected: the corresponding deviation at the electron detector is lower than 1 *mm*. So the electron detector will see the bremsstrahlung electron in the energy range covered by the sensitive area.

# Chapter 3

# The measurement of the experimental asymmetry

In this chapter we will explain the method used to measure the experimental asymmetry $A_{exp}$ and how we extract it from the data.

Furthermore, we will explain how the systematic errors are reduced by taking data of left and right events of photon polarization states. We will also see how to measure the dilution of our Compton signal by taking data when the cavity isn't locked. And finally, the data taking procedure will be described.

## 3.1 Principle of the experimental asymmetry extraction

The number of events for each electron polarization state is defined by :

$$N^{\pm} = r^{\pm}T^{\pm} \qquad \text{with } r^{\pm} = \mathcal{L}_s^{\pm}\sigma_s^{\pm} + \mathcal{L}_b^{\pm}\sigma_b^{\pm}$$

where, for each helicity gate, $r^{\pm}$ is the rate of events, $T^{\pm}$ the duration of a polarization state ($\sim 30\,ms$ for a $30\,Hz$ beam helicity flip), $\mathcal{L}_{s,b}^{\pm}$ is the luminosity at the CIP for the Compton signal (Cavity locked) and the background (Cavity OFF) and $\sigma_{s,b}^{\pm}$ the correspondent cross sections.

The raw asymmetry for the number of events is thus :

$$A_{raw}^{N} = \frac{N^+ - N^-}{N^+ + N^-} = \frac{r^+T^+ - r^-T^-}{r^+T^+ + r^-T^-}$$

Let us define the time $A_T$ and rate $A_r$ asymmetries :

$$A_T = \frac{T^+ - T^-}{T^+ + T^-} \qquad A_r = \frac{r^+ - r^-}{r^+ + r^-}$$

It yields:

$$A_{raw}^{N} = \frac{A_T + A_r}{1 + A_T A_r}$$

However if the time of data taking is different between the two beam helicity states, the raw asymmetry will be biased by the time asymmetry $A_T$. It is the same way for the charge asymmetry of the electron beam.

So those two parameters have to be measured during the run for each state of polarization. In order to avoid to introduce false asymmetries and dilution of our experimental asymmetry, we must normalize the number of events detected to the time of acquisition and to the beam intensity.

Hence, we will introduce the normalized rates (in $kHz/\mu A$) $r^{\pm} = \frac{N^{\pm}}{T^{\pm}I^{\pm}}$and the corresponding raw asymmetry :

$$A_{raw} = \frac{\frac{N^+}{T^+I^+} - \frac{N^-}{T^-I^-}}{\frac{N^+}{T^+I^+} + \frac{N^-}{T^-I^-}}$$

However, the signal we get is diluted by the background. So the experimental asymmetry is given by :

$$A_{exp} = dil.A_{raw}$$

and this for each state of the photon beam polarization.

The dilution is defined as follows : $dil \doteq (1 + \rho)$ where $\rho = b/s$ and $b$ is the background and $s$ the pure signal.

But we don't have access to the pure signal $s$, we only know $B$ and $S$ where $B = b = \frac{1}{2}\left(\frac{N^+}{T^+I^+} + \frac{N^-}{T^-I^-}\right)$ when the cavity is OFF and $S = s + b = \frac{1}{2}\left(\frac{N^+}{T^+I^+} + \frac{N^-}{T^-I^-}\right)$ when the cavity is ON. So $\rho = b/s = \frac{B/S}{1-B/S}$ and then $dil = \frac{1}{1-B/S}$.

Thus, for each state of the cavity and if we neglect the false asymmetries of position we can calculate the polarization of the electron beam by :

$$A^{L,R} = dil_{L,R} A_{exp}^{L,R}$$

### 3.1.1 False asymmetries

Now we will study the false asymmetry induced by a helicity correlated variation of the $Y$ position of the electron beam in the cavity.

If the vertical position of the beam is drifting, the counting rates seen in the two detectors will vary. This is due to the variation of the luminosity at the CIP.

The asymmetry without dead time and current corrections is:

$$N^+ = \frac{1+A}{2}(N^+ + N^-) = N_0(1 + A)$$
$$N^- = \frac{1-A}{2}(N^+ + N^-) = N_0(1 - A)$$

where $N_0$ is the average counting rates between two states of electron beam helicity.

For example, the counting rates of helicity $-$ will pass from $N^-$ to $N^- + \Delta N$ where $\Delta N = \frac{\partial N}{\partial Y}\Delta Y$ and $\Delta N \ll N^+, N^-$, if the vertical position of the electron beam changes between two states of helicity.

Thus the asymmetry becomes:

$$A_{exp} = \frac{N^+ - (N^- + \Delta N)}{N^+ + N^- + \Delta N} = A_{phys} - \frac{\Delta N}{2N_0}$$

So we can deduce the false asymmetry of position $F_A$ :

$$F_A = \frac{1}{N_0}\frac{\Delta Y}{2}\frac{\partial N}{\partial Y}$$

where :

- $\frac{\Delta Y}{2}$ is the difference of position correlated to the flip of helicity.
- $\frac{\partial N}{\partial Y}$ is the sensibility efficiency of the detector to the asymmetry of position (*cf* Figure 3.1).
- $N_0$ is the counting rate corresponding to the average position between the two states.

All these quantities can be determined with the so called "bell curve" (See Section 3.2).

## 3.2 Data taking procedure

This section explains the procedure to take runs with the Compton polarimeter.

The very first step is to check if the laser is ON, if the photon detector is in the data taking position and if the electron detector is in the so called "beam stream" position, that is on the path of the scattered electrons.

Then we have to a get a good crossing of the photon and electron beams. For this, we remind that the cavity can not be moved. As a consequence, we have to move the electron beam vertically to optimize the luminosity: this procedure is called a vertical scan. This is performed by modifying the field in the four coupled dipoles. The table below shows the correspondence between field variations in the dipoles and vertical position variations of the electron beam and this for different energies of the electron beam. In other words, if we want to scan the luminosity by steps of 25 $\mu m$ with an incident beam energy of 4 $GeV$, we have to modify the field in the dipoles by steps of 50 $G.cm$.

| Step 25 $\mu m$ | Step 100 $\mu m$ | Energy |
|---|---|---|
| 10 $G.cm$ | 40 $G.cm$ | 0.8 $GeV$ |
| 20 $G.cm$ | 80 $G.cm$ | 1.6 $GeV$ |
| 30 $G.cm$ | 120 $G.cm$ | 2.4 $GeV$ |
| 40 $G.cm$ | 160 $G.cm$ | 3.2 $GeV$ |
| 50 $G.cm$ | 200 $G.cm$ | 4.0 $GeV$ |
| 60 $G.cm$ | 240 $G.cm$ | 4.8 $GeV$ |
| 70 $G.cm$ | 280 $G.cm$ | 5.6 $GeV$ |

Hence we can scan over a few millimeters without any noticeable modification of the beam position on the Hall A target. During this scan, the counting rates increase, reach a maximum and then decrease, following the "bell curve" distribution. The maximum of the curve is the optimal crossing between the two beams. After activating a magnetic feedback procedure to lock the vertical position of the electron beam, we can finally take data.

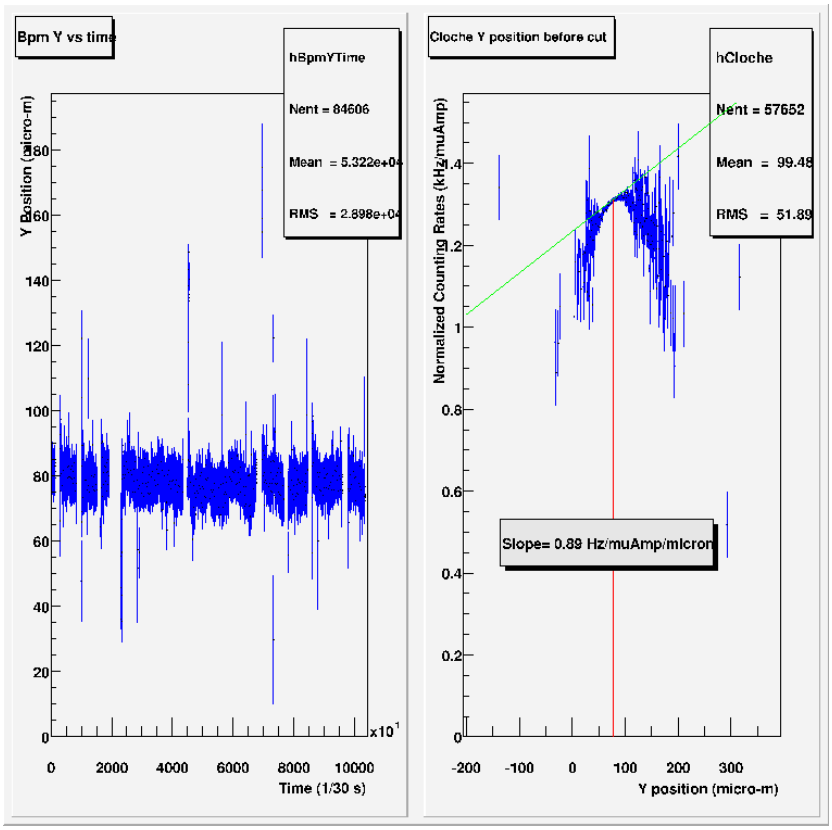


Figure 3.1: On the left graph is plotted the vertical position of the electron beam during the run. On the right is shown the normalized counting rates versus the vertical position: the so called "bell curve". The red line represents the mean position of the beam during the data taking and the green one the sensibility to the false asymmetries induced by the helicity correlated variations of the vertical position. When the beam is at a position corresponding to the top of the "bell curve", we are less sensitive to false asymmetries of position. Let us notice that we can also measure the spot size of the electron beam: it is twice the RMS of the "bell curve".

A run of the Compton polarimeter is composed in 4 sequences:

- Cavity OFF ($\sim$30 *sec*) for background measurement.

- Cavity ON with RIGHT circularly polarized photons ($\sim$100 *sec*) for asymmetry measurement.
- Cavity OFF ($\sim$30 *sec*) for background measurement.
- Cavity ON with LEFT circularly polarized photons ($\sim$100 *sec*) for asymmetry measurement.

This pattern is repeated during all the run and automated by the data acquisition.

## 3.3 Analysis program of the electron detector

In this section we will see details of the electron detector analysis program. We will first explain the use of each program and then explicitly explain what do each one. All the programs of the analysis of the electron detector data are written in C++/ROOT[9]. The old program based on the analysis of the photon detector was sensitive to the threshold determination ("Compton edge") as well as the resolution efficiency. I wrote programs which generate control histograms in order to implement more easily this important improvement.

### 3.3.1 Event selection

The first program characterizes the data :

- check if the cavity is ON or OFF.
- cut each 60 first events of each gate of cavity status (ON or OFF) because the state of the cavity may be undetermined.
- cut on the helicity status of the electron beam because the state of the charge is undetermined during the spin flip.
- cut on the current with a threshold of 4 $\mu A$.
- cut on the vertical position of the electron beam.

The cut on the position is made using the distribution of the vertical position. For RIGHT and LEFT photon polarization, the Y position has to be within 20 $\mu m$ around the mean of the distribution. Hence, we should have the same false asymmetry for RIGHT and LEFT.

### 3.3.2 Asymmetry calculation

The second program allows us to extract the polarization from the calculation of the experimental asymmetry. It performs this on the events previously selected.

First it determines the live time of the acquisition. To do so, it divides the number of events stored by the scalers (not dead time sensitive). Then it normalizes the number of good electron events to the beam intensity.

In the next step, the strip maps of each plane are filled. For each strip we store the normalized counting rate acquired for each laser helicity gate (see Figure 3.2):

$$\frac{1}{I.T}\frac{(N^+ + N^-)}{2}$$

where $I$ and $T$ are the average of respectively beam intensity and lifetime for each electron beam helicity status.

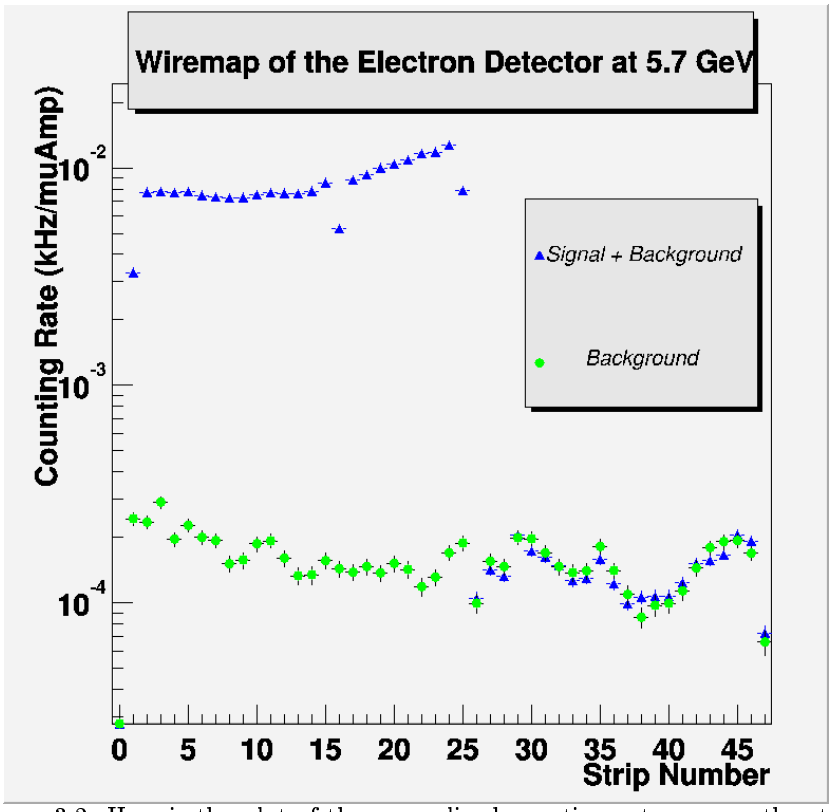


Figure 3.2: Here is the plot of the normalized counting rates versus the strip number of the plane. We get this plot for each of the three planes actually in use of the electron detector.

Then, it calculates the asymmetry between the normalized counting rates for each strip of each plane, in other words :

$$A_{raw}^{L,R} = \frac{\frac{N^+}{I^+T^+} - \frac{N^-}{I^-T^-}}{\frac{N^+}{I^+T^+} + \frac{N^-}{I^-T^-}}$$

Afterwards, it uses informations on the cavity status (ON/OFF) to correct for dilution effects in each strip of the plane. So, it can retrieve the experimental

asymmetry:

$$A_{exp}^{L,R} = dil_{L,R} A_{raw}^{L,R}$$

where $dil_{L,R} = \left(1 - \frac{B^{L,R}}{S^{L,R}}\right)^{-1}$ and the error on this dilution is [10]:

$$d(dil_{L,R}) = \frac{dil_{L,R}^2}{S^{L,R}} \frac{1}{\sqrt{(dB^{L,R})^2 + \left(\frac{B^{L,R}}{S^{L,R}}\right)^2 . (dS^{L,R})^2}}$$

Then it fills a same histogram (the so called "Wide Plane") with the asymmetries left and right (cavity status) of each plane successively. The program fits this histogram with the theoretical asymmetry to determine the energy calibration ($Y_{det}$ and "Compton edge") and the beam polarization (see Figure 3.3).

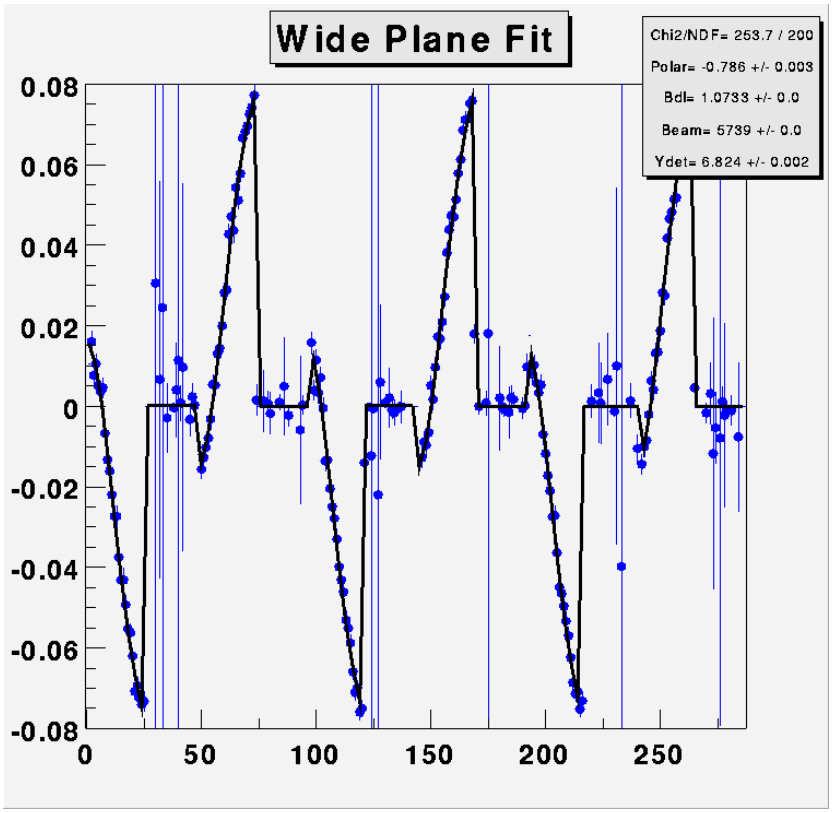


Figure 3.3: This plot shows the fit of the experimental asymmetries. The asymmetry is in ordinate and the cumulate strip number in X-coordinate. We filled this histogram with, for each plane the right and left asymmetries (corresponding to the right and left photon helicity).

We plotted on the graph below the experimental asymmetry versus the strip number for the plane B.

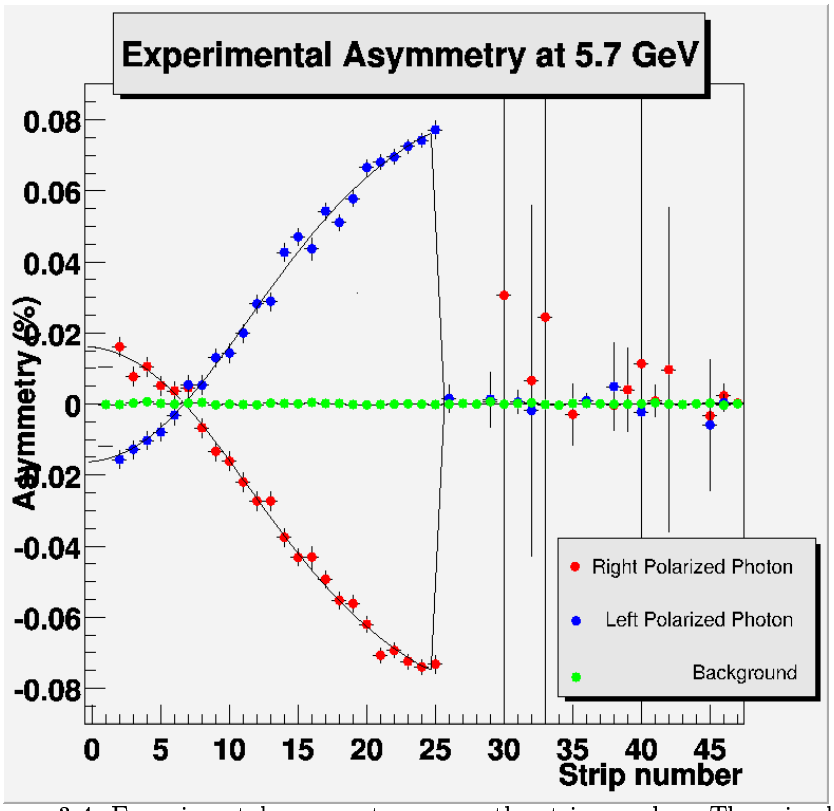


Figure 3.4: Experimental asymmetry versus the strip number. There is also the fit by the $A_{th}(\rho)$ function.

# Chapter 4

# Preliminary results of polarization measurement

In this chapter, we will give the results of the beam polarization measurement during the summer 2001. We will first approach the data retrieved during $A_1^n$ and then those of $g_2^n$ (at least until I was at JLab).

## 4.1 Polarization during E99-117

The histogram below show the polarization measurements I took from June 7th to July 31st.

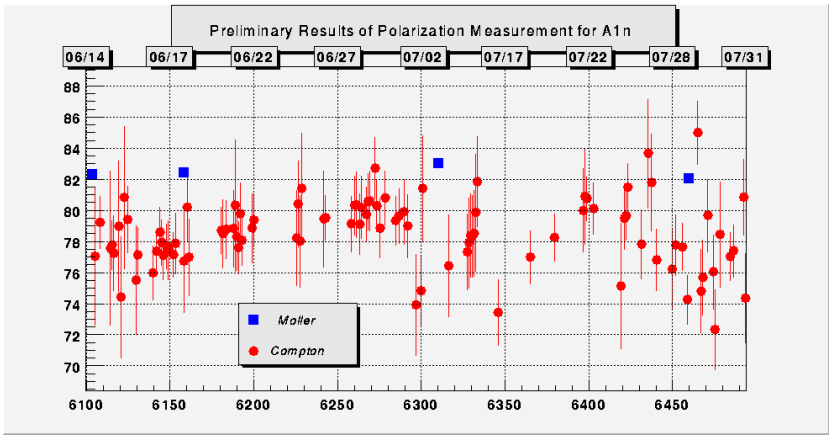


Figure 4.1: The polarization of the electron beam during the $A_1^n$ experiment. The systematic error on the Moeller measurement is $err_{syst} = 2.4\%$.

## 4.2 Polarization during E97-103

The histogram below summarizes the polarization measurements I took from August 1st to August 30th. The data taken during the two first parts of the experiment ($E = 3.4\,GeV$ and $E = 4.6\,GeV$) are not shown because the electron detector received Compton signal on only the eight first strips at $E = 3.4\,GeV$. As a consequence, the fit on this data isn't reliable because of the lack of constraints on it.

For the kinematic $E = 4.6\,GeV$, the beam was mistuned after the dipole $D_3$, resulting in a huge background in the detector. Hence, the Compton signal was completely diluted by this background.

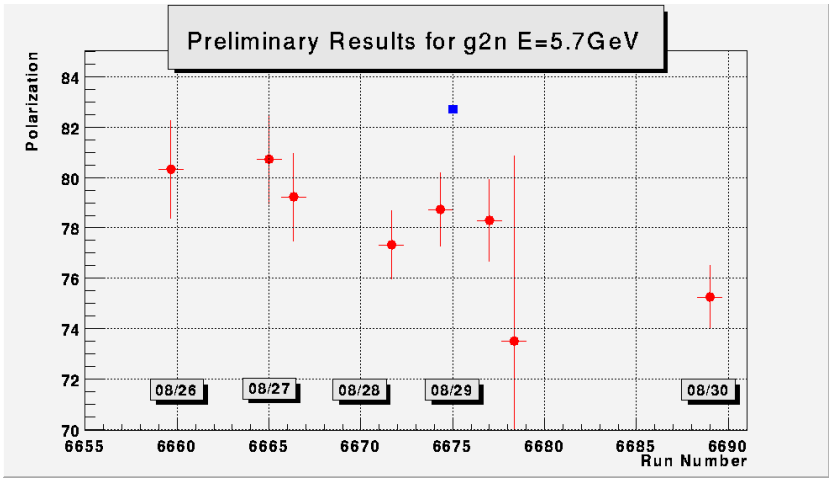


Figure 4.2: The polarization of the beam during the kinematic $E = 5.7\,GeV$ of the $g_2^n$ experiment. The Compton measurement are in red circles and Moeller in blue squares.

# Conclusion

We described in the second chapter all the main components of the Compton polarimeter and the constraints on it in order to retrieve a polarization measurement. We then explained how to get the polarization measurement from the raw asymmetries. Hence we noticed that to be able to get a measurement, a good tune of the beam is required (halo of the beam, vertical position inside the chicane) as well as a beam stability during the data taking. So the Compton operator has a lot of parameters to take into account in order to insure a reliable measurement of the beam polarization.

Therefore, during $A_1^n$ the beam was quite good most of the time. For $g_2^n$, the kinematics (at $E = 3.4\,GeV$) didn't favor a measurement of the polarization with the electron detector, but we have the data of the photon detector. For $E = 4.6\,GeV$, the electron detector was flooded by a huge background maybe induced by a mistune of the beam after the third dipole or a non-optimal vacuum. Nevertheless, we will be able to retrieve data with the electron detector until the end of this experiment.

To conclude, the automatic analysis program of the electron detector generates now histograms to control the quality of the data we are taking and is faster than the one written in the FORTRAN framework. Moreover, this program is not sensitive to the threshold determination neither to the resolution efficiency. Hence it is an important improvement for the on-line monitoring of the beam polarization.

# Acknowledgments

First I would like to thank Jean Castor who offered me the great opportunity to come at JLab. I would like also to thank Helene Fonvieille and Jean Orloff for their support during the long way to get a visa. Without them I wouldn't have had the opportunity to make my internship at JLab, which have been a great experience from all points of view.

On the American side, I would like to thank Gordon Cates and the University of Virginia for hiring me as a research assistant and giving me compensations for these four months of training. I acknowledge all the "Cates lab" gang which made my arrival at UVa easy and pleasant, especially Jaideep.

I would like to thank Alexandre Deur who gave me the opportunity to work on the Compton polarimeter and take responsibilities and an active part in the $A_1^n$ and $g_2^n$ experiments. I really enjoyed working at JLab and I learned a lot. I would like to thank all the Saclay group, David Lhuillier, Damien Neyret, Thierry Pussieux, Fréderic Marie and Etienne Burtin who allowed me to work on the Compton polarimeter. They have been always very friendly. On the JLab side, I acknowledge the $^3He$ group and above all: Jian-Ping Chen and Wolfgang Korsch.

Finally, I would like to thank all the "french connection": Matthieu (SOS C++), Antoine, Antonin, Jason, Olivier, Christophe, Julie and Yves who participated in making my life pleasant at JLab.

# Bibliography


[1] J.P. Chen, Z.-E. Meziani, P.A. Souder *et al.* Precision measurement of the neutron asymmetry $A_1^n$ at large $x_B$ using TJNAF at 6 $GeV$. PR 99-117 (1999).

[2] E99-117 web site. http://hallaweb.jlab.org/physics/experiments/he3/A1n/index.html

[3] T. Averett, W. Korsch *et al.* Search for higher twist effects in the neutron spin structure function $g_2^n\left(x, Q^2\right)$. PR 97-103 (1997).

[4] E97-103 web site. http://hallaweb.jlab.org/physics/experiments/he3/g2/temp/general.html

[5] A. Deur. Etude expérimentale de la structure en spin du neutron $\left({}^3He\right)$ à bas $Q^2$ : une connexion entre les règles de sommes de Bjorken et Gerasimov-Drell-Hearn. Thèse de l'Université Blaise Pascal (2000).

[6] C.S. Wu *et al.* Phys. Rev. Serie II vol 105, pp1413-1415 (1957); C.S. Wu, Rev. Modern Phys. vol 31, pp783-790 (1959).

[7] M. Baylac. Mesure de la polarisation du faisceau d'électrons du Jefferson Laboratory par effet Compton pour l'expérience HAPPEX en diffusion élastique électron-proton. Thèse de l'Université Claude Bernard - Lyon I (2000)

[8] G. Bardin, C. Cavata, B. Frois *et al.* Conceptual design report of a Compton polarimeter for CEBAF Hall A. http://www.jlab.org/compton/Documentation/1996/proposal.ps.gz (1996)

[9] The ROOT web site. http://root.cern.ch

[10] Discussions with David Lhuillier and Fréderic Marie.

[11] M. Baylac. Characterization of the PbWO4 crystals for the photon detector of the Compton Polarimeter at the Jefferson Laboratory.

[12] CMS detector web site. http://d.home.cern.ch/d/denes/www/cms_detector.htm